Considerations on the control design for a three-tether wave energy converter

N.Y. Sergiienko[a,*], B.S. Cazzolato[a], M. Arjomandi[a], B. Ding[a], L.S.P. da Silva[b]

[a] *The University of Adelaide, School of Mechanical Engineering, Adelaide, Australia*
[b] *University of São Paulo, Department of Naval Architecture and Ocean Engineering, São Paulo, Brazil*

Abstract

Wave energy converters (WECs) capable of extracting power in multiple degrees of freedom require a special attention from control engineers as the control problem becomes multivariable involving highly coupled dynamics of the plant. Taking the three-tether submerged buoy as an example of a multi-degree-of-freedom WEC, this paper presents three main steps that should be taken during control system development. Firstly, an understanding of the system dynamics, its rigid body modes of vibration and input/output controllability is built using the singular value decomposition approach. Then, a causal close-to-optimal controller developed for the single-tether heaving WEC is extended to the multivariable control problem, demonstrating a significant increase in the power output as compared to the simple spring-damper approach. At the final stage, technical requirements imposed by this controller on the power take-off (PTO) machinery are investigated showing that, in order to achieve a 15%-improvement in power absorption compared to a quasi-standard spring-damper control, the amount of reactive power should be increased by 50%, forcing one PTO unit to operate as an actuator all the time.

Keywords:
multivariable control; power take-off; three-tether WEC; wave energy converter

1. Introduction

The power production of an oscillating wave energy converter is directly dependent on its hydrodynamic properties and its interaction with an incoming wave front. The latter is determined by the control system design which defines whether the buoy passively follows waves or is actively controlled to harvest more energy. Therefore, a properly designed control system of the WEC can increase the productivity several times (Hals et al., 2011) in comparison to a passive control load.

The majority of proposed control algorithms developed for WECs are for systems that operate in one degree of freedom and are considered as single-input-single-output (SISO) systems (e.g. Hardy et al. (2016); Ding et al. (2016); Faedo et al. (2017)). However, more energy can be harvested when several degrees of freedom are involved and coupled to the power take-off unit (Falnes, 2002a). It is generally assumed that any SISO controller can be easily extended and applied to the multivariable WEC, which is true when there is an independent control effort over each mode of oscillation as shown in (Zou et al., 2017; Abdelkhalik et al., 2017; Korde et al., 2017). In the case when the PTO system has an operational space different from the wave-induced motion of the WEC (e.g. NEMOS GmbHs (2017)), all degrees-of-freedom become coupled through the PTO and mooring system. Such WECs require more complex multiple-input-multiple-output (MIMO) control algorithms which take into account interactions in the system dynamics.

Regardless of whether the converter operates in one or several degrees of freedom, its control is generally considered as an optimisation problem with the objective to maximise power generation subject to displacement and/or load force constraints (Ringwood et al., 2014). However, the design of the WEC is not only driven by the maximisation of the energy production but takes into consideration the cost of the delivered electricity accounting for the capital and operational expenditures of the system. Therefore, improved performance of the WEC from an advanced control law is almost always associated with a more complex design of the power take-off machinery. For example, the model predictive control outperforms other controllers in terms of the absorbed power, but it requires the highest peak-to-average ratio of the power flowing through the PTO (Hals et al., 2011).

Therefore, recently, more attention has been brought to the practical side of the development and implementation of the WEC control systems. Sandia National Laboratories (Wilson et al., 2016; Coe et al., 2017) have performed extensive research on the assessment of the most common control strategies, where the comparison has been done not only in terms of the power output but also involving other performance indices related to the PTO capacity requirements. The results have demonstrated that

*Corresponding author
Email address: nataliia.sergiienko@adelaide.edu.au (N.Y. Sergiienko)

PTO specifications, such as the required energy storage, the maximum slew rate of the load force, etc., significantly vary depending on the control strategy. Furthermore, the implemented controller should account for practical limitations of the power take-off as demonstrated by Genest et al. (2014); Nie et al. (2016), where the transmission energy losses and efficiency of the machinery are included in the formulation of the control law. Therefore, at the early stage of the WEC development, the PTO machinery should be designed according to the requirements imposed by the selected control strategy, and if not possible, the controller should take into account technical constraints of the system.

The current paper addresses two research questions: (i) how to modify the SISO controller for the WEC that operates with multiple degrees of freedom? and (ii) what challenges may arise when it is required to implement the close-to-optimal controller in practice? The description of the converter, its numerical model and the controllability analysis are presented in Section 2. The design of the high- and low-level control loops and the performance of the suggested control strategy are shown in Section 3. The possibility of practical application of optimal control and associated specifications and requirements for the power take-off machinery are discussed in Section 4.

2. Wave energy converter

2.1. System description

The WEC considered in this study is a fully submerged disk-like buoy connected to three power take-off units by means of the flexible tethers as shown in Figure 1. Such configuration of the PTO allows the extraction of power from surge, heave and pitch motions simultaneously. All parameters and dimensions of the converter have been selected such that the cost of electricity is minimised considering that the PTO is capable of generating a force proportional to the tether displacement and velocity (spring-damper control).

2.2. Dynamic model

This WEC has six degrees-of-freedom, so its motion can be described by the position vector $\mathbf{x} \in R^{6\times1}$ (x_1 surge, x_2 sway, x_3 heave, x_4 roll, x_5 pitch, x_6 yaw) in the reference (Cartesian) coordinate frame $Oxyz$. The buoy is connected to three tethers that are represented by the a vector of tether length variables $\mathbf{q} = [l_1 \quad l_2 \quad l_3]^\mathsf{T}$. The kinematic relationship between the buoy velocity $\dot{\mathbf{x}}$ and the rate of change of the tether length has a form $\dot{\mathbf{q}} = \mathbf{J}^{-1}(\mathbf{x})\dot{\mathbf{x}}$, where $\mathbf{J}^{-1}(\mathbf{x}) \in R^{3\times6}$ is the inverse kinematic Jacobian which is a function of the buoy current position (Sergiienko et al., 2018).

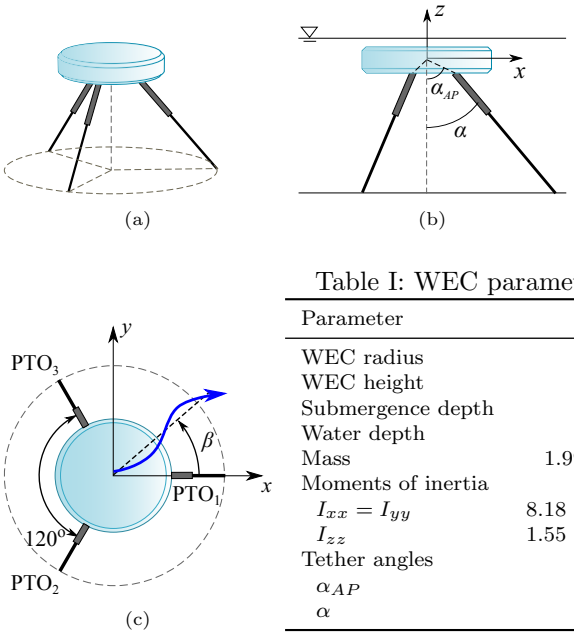

Table I: WEC parameters.

Parameter	Value
WEC radius	12.5 m
WEC height	5 m
Submergence depth	2 m
Water depth	30 m
Mass	1.99×10^6 kg
Moments of inertia	
$I_{xx} = I_{yy}$	8.18×10^7 kg·m^2
I_{zz}	1.55×10^8 kg·m^2
Tether angles	
α_{AP}	65°
α	40°

Figure 1: Geometry and parameters of the three-tether wave energy converter: (a) 3D view, (b) front view, (c) top view. The angle β shows the direction of the wave propagation.

2.2.1. Full dynamics

The motion of the three-tether WEC can be described by the following equation:

$$\mathbf{M}\ddot{\mathbf{x}} = \mathbf{F}_{exc} + \mathbf{F}_{rad} + \mathbf{F}_{visc} + \mathbf{F}_{buoy} + \mathbf{F}_{tens}, \qquad (1)$$

where

- $\mathbf{F}_{exc}$ is the wave excitation force vector;
- $\mathbf{F}_{rad}$ is the wave radiation force vector modelled as:

$$\mathbf{F}_{rad} = -\mathbf{A}_\infty\ddot{\mathbf{x}} - \int_0^t \mathbf{K}_{rad}(t-\tau)\dot{\mathbf{x}}(\tau)d\tau \equiv -\mathbf{A}_\infty\ddot{\mathbf{x}} - \mathbf{F}_r, \qquad (2)$$

where $\mathbf{A}_\infty$ is the matrix with infinite frequency added mass coefficients, and $\mathbf{K}_{rad}(t)$ is a retardation function, and $\mathbf{F}_r$ is replaced by the state-space model using the Marine System Simulator toolbox developed by Perez and Fossen (2009):

$$\dot{\mathbf{p}}_r = \mathbf{A}_r\mathbf{p}_r + \mathbf{B}_r\dot{\mathbf{x}}, \qquad (3)$$

$$\mathbf{F}_r = \mathbf{C}_r\mathbf{p}_r. \qquad (4)$$

Here $\mathbf{p}_r \in R^{36\times1}$ is an auxiliary vector without any physical meaning (for details see Sergiienko et al. (2017)), $\mathbf{A}_r$, $\mathbf{B}_r$, and $\mathbf{C}_r$ are the state space matrices. The frequency-dependent coefficients of the excitation and radiation forces are obtained using WAMIT (Lee, 1995);

- $\mathbf{F}_{visc}$ is a viscous damping force given by

$$\mathbf{F}_{visc} = -\frac{1}{2}\rho \mathbf{C}_d \mathbf{A}_d \|\dot{\mathbf{x}}\| \dot{\mathbf{x}}, \tag{5}$$

where $\mathbf{C}_d$ and $\mathbf{A}_d$ are the matrices of the drag coefficients and the cross-section areas of the buoy perpendicular to the direction of motion respectively. Drag coefficients are taken as $C_{d,x} = C_{d,y} = 0.7$, $C_{d,z} = 1.28$ and $C_{d,xz} = 0.22$. These values were calculated from the numerical wave tank experiments (Rafiee and Fievez, 2015) for similar buoy geometry;

- $\mathbf{F}_{buoy}$ is the buoyancy force

$$[0 \quad 0 \quad (m_w - m_b)g \quad 0 \quad 0 \quad 0]^\mathsf{T}, \tag{6}$$

where m_w is the mass of the displaced water, and m_b is the mass of the WEC;

- $\mathbf{F}_{tens}$ is the generalised tether force in the Cartesian coordinate frame $Oxyz$

$$\mathbf{F}_{tens} = \mathbf{J}^{-\mathsf{T}} \mathbf{F}_t = \mathbf{J}^{-\mathsf{T}} (\mathbf{F}_{t0} + \mathbf{F}_u), \tag{7}$$

and the vector of tether forces $\mathbf{F}_t \in R^{3\times 1}$ is a superposition of the initial tension in the tethers that counteracts the buoyancy force, and of the control forces exerted on the buoy from the PTO machinery. Also, the tethers are assumed to be flexible and they can become slack which is modelled as $F_{t,i} = \min(F_{t0,i} + F_{u,i}, 0)$.

The presence of the viscous drag term ($\mathbf{F}_{visc}$) and generalised tether force ($\mathbf{F}_{tens}$) makes the system (1) nonlinear with respect to $\mathbf{x}$ and $\mathbf{F}_u$. Therefore, for the control system development, Equation (1) should be represented in a state-space form, and, therefore, linearised.

2.2.2. Linearised state-space model

The approximation of the viscous damping force by its linear analogue is done using a Lorenz linearisation approach suggested by Folley (2016). Thus, $\mathbf{F}_{visc} \approx -\mathbf{B}_v \dot{\mathbf{x}}$, where the diagonal elements of the linearised damping matrix $\mathbf{B}_v \in R^{6\times 6}$ are obtained using the iteration procedure described by Bacelli et al. (2013). For the WEC detailed in Table I this method gives $B_{v,1} = B_{v,2} = 2.8 \times 10^5$ N·s/m, $B_{v,3} = 1.9 \times 10^5$ N·s/m and $B_{v,4} = B_{v,5} = 2 \times 10^7$ N·s/rad.

Nonlinearities in the generalised tether force are associated with the inverse kinematic Jacobian, which is position-dependent. So, the approximated tether force is:

$$\mathbf{F}_{tens} \approx -\mathbf{K}_t \mathbf{x} + \mathbf{J}_0^{-\mathsf{T}} \mathbf{F}_u, \tag{8}$$

where $\mathbf{K}_t$ can be found in Scruggs et al. (2013) and $\mathbf{J}_0^{-1} = \mathbf{J}^{-1}(\mathbf{x}_0)$ is the inverse kinematic Jacobian at the nominal position of the buoy $\mathbf{x}_0 = \mathbf{0}_{6\times 1}$.

As a result, the linearised state-space model of the WEC can be written as:

$$\begin{aligned}
\dot{\mathbf{X}} &= \left[\begin{array}{c} \dot{\mathbf{x}} \\ \ddot{\mathbf{x}} \\ \hline \dot{\mathbf{p}}_r \end{array}\right] = \\
&= \left[\begin{array}{cc|c} \mathbf{0}_{6\times 6} & \mathbf{I}_{6\times 6} & \mathbf{0}_{6\times 36} \\ -(\mathbf{M}+\mathbf{A}_\infty)^{-1}\mathbf{K}_t & -(\mathbf{M}+\mathbf{A}_\infty)^{-1}\mathbf{B}_v & -(\mathbf{M}+\mathbf{A}_\infty)^{-1}\mathbf{C}_r \\ \hline \mathbf{0}_{36\times 6} & \mathbf{B}_r & \mathbf{A}_r \end{array}\right] \left[\begin{array}{c} \mathbf{x} \\ \dot{\mathbf{x}} \\ \hline \mathbf{p}_r \end{array}\right] + \left[\begin{array}{c} \mathbf{0}_{6\times 6} \\ (\mathbf{M}+\mathbf{A}_\infty)^{-1} \\ \hline \mathbf{0}_{36\times 6} \end{array}\right] \left(\mathbf{F}_{exc} + \mathbf{J}_0^{-\mathsf{T}} \mathbf{F}_u\right) \\
&\equiv \mathbf{A}_{\text{WEC}} \mathbf{X} + \mathbf{B}_{\text{WEC}} \mathbf{U}, \\
\mathbf{Y} &= \dot{\mathbf{x}} = \left[\begin{array}{c|c|c} \mathbf{0}_{6\times 6} & \mathbf{I}_{6\times 6} & \mathbf{0}_{6\times 36} \end{array}\right] \mathbf{X} = \mathbf{C}_{\text{WEC}} \mathbf{X},
\end{aligned} \tag{9}$$

and the transfer function that corresponds to this model is:

$$\mathbf{G}(s) = \mathbf{C}_{\text{WEC}} (s\mathbf{I} - \mathbf{A}_{\text{WEC}})^{-1} \mathbf{B}_{\text{WEC}}. \tag{10}$$

The nonlinear model in Equation (1) is used to assess the controller performance, while the controller design is based on the linearised model in Equation (9).

2.2.3. Implementation

The time-domain simulations are implemented in MATLAB/Simulink with a time step of 0.01 s using the ode45 solver. Where the power assessment is required, simulation time is set to $300 \times T_p$ seconds while the first $15 \times T_p$ are not taken into account due to the transient effects. T_p is the peak period of the modeled irregular wave.

2.3. Controllability

The converter shown in Figure 1 belongs to the class of underactuated mechanisms as it has six degrees-of-freedom (DOF) but only three independent control inputs (non-square plant). In order to identify what DOFs can be controlled and quantify interactions in this MIMO system, the transfer function of the WEC $\mathbf{G}(j\omega) \in R^{6\times 3}$ should be decomposed using singular value decomposition (SVD):

$$\mathbf{G}(j\omega) = \mathbf{U}\mathbf{\Sigma}\mathbf{V}^H, \tag{11}$$

where $\mathbf{U} \in R^{6\times6}$ and $\mathbf{V} \in R^{3\times3}$ are the singular vectors that form orthonormal bases for the output and input space, correspondingly, and $\mathbf{\Sigma} \in R^{6\times3}$ is a diagonal matrix with three non-negative singular values $\sigma_1 \geq \sigma_2 \geq \sigma_3$.

Singular vectors $\mathbf{U}$ correspond to the six rigid body modes of vibration (not to be confused with hydrodynamic modes) each of which has its own natural frequency and mode shape (Fu and He, 2001). In other words, vibration modes can be explained as follows. The motion of the WEC is usually described using conventional rigid-body modes, or DOFs, such as surge, sway, heave, roll, pitch and yaw. However, these DOFs are not independent in the three-tether WEC, but are coupled (i) hydrodynamically due to the cylindrical shape of the buoy, and (ii) through inclined mooring lines. Coupled DOFs that oscillate with the same natural frequency form a mode of vibration (Ding et al., 2019).

The graphical representation of the mode shapes that correspond to $U_i\,(i = 1\ldots6)$ are shown in Figure 2. Since the system has three control inputs, only the first three modes out of the six, namely U_1, U_2, and U_3 can be actively controlled by the power take-off machinery. It can be seen that both output modes U_1 and U_4 involve buoy motion in surge and pitch, but:

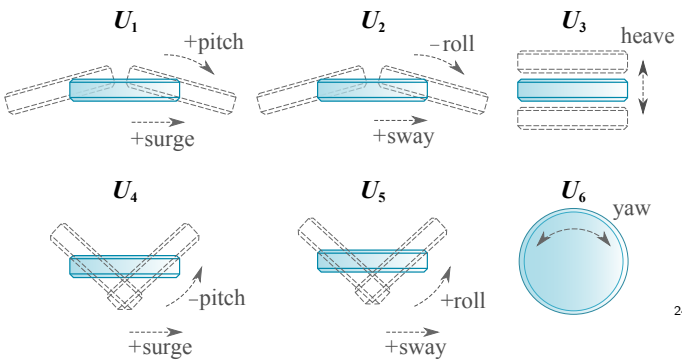

Figure 2: Graphical representation of the rigid body modes of the three-tether WEC.

(i) U_1 has a lower resonant frequency than U_4. The incoming wave will excite the buoy motion in either mode U_1 or U_4 depending on which resonant frequency is closer to the wave frequency;

(ii) surge and pitch modes are included in U_1 and U_4 with different phases and amplitudes. While U_1 is dominated by surge motion, U_4 is dominated by pitch. Moreover, surge and pitch modes are in phase in U_1, and have opposite phases in U_4;

(iii) U_1 is controllable while U_4 is not. U_4 can be excited by the incident wave, but the PTO machinery has no effect on this mode.

Another important information obtained from the SVD is related to the singular values $\sigma_j (j = 1\ldots3)$. In control theory, singular values are used to show the output directions in which the system inputs are most effective (Skogestad and Postlethwaite, 2007) and to identify any controllability problems in the plant. The frequency-dependent singular values of the WEC which correspond to the controllable modes $U_i\,(i = 1\ldots3)$ are demonstrated in Figure 3a. It is clear from the plot that in the frequency range of $0.5-0.75$ rad/s (wave period $8-12$ s) the coupled surge/pitch U_1 and sway/roll U_2 modes have singular values an order of magnitude higher than these for heaving mode U_3. This implies that less effort is required to control the buoy in surge and sway than in heave at this range of frequencies. Moreover, if the ratio between the maximum and minimum singular values (condition number) is larger than 10, inverse-based controllers may be sensitive to 'unstructured' input uncertainty which is undesirable for practical applications (Skogestad and Postlethwaite, 2007).

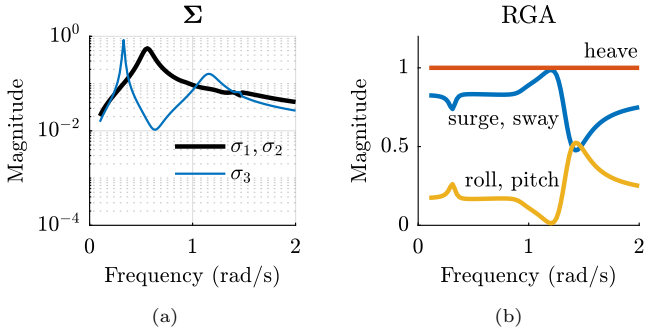

Figure 3: Controllability measures of the three-tether WEC: (a) singular values, and (b) Relative Gain Array.

Another measure which is widely used to identify control properties of the plant is the Relative Gain Array $\mathrm{RGA}(G) = \Lambda(G) \triangleq G \circ (G^{-1})^{\mathsf{T}}$, where $\circ$ denotes the Hadamard product (element-by-element multiplication). The RGA is mostly used to determine an effective input-output pairing for use in the control design, and to indicate outputs with poor controllability. So, if the sum of the elements in a row of RGA is small ($\ll 1$), then the corresponding output cannot be controlled. The RGA matrix of the three-tether WEC is $\Lambda(G) \in R^{6\times3}$, where six rows represent the WEC DOFs (outputs) and three columns correspond to the three control inputs through the tethers. In order to demonstrate the controllability property of each DOF, the RGA matrix of the plant is calculated over the range of frequencies $\Lambda\,(G(\omega))$ and row sums that correspond to these DOFs are shown in Figure 3b. As a result, relatively large RGA elements (> 0.5) indicate that the PTO system has a strong control authority in surge, sway and heave, but poor controllability over pitch and roll (values are < 0.5).

However, it should be noted that this analysis has been performed for the nominal position of the buoy $\mathbf{x}_0 = \mathbf{0}_{6\times1}$; and the control property of this WEC is subject to the buoy orientation.

3. Controller design and performance

In this section, the 'simple but effective' velocity tracking controller developed by Fusco and Ringwood (2013) is extended to the multivariable system. As shown in Figure 4, the control structure has two major loops: (i) a high level loop sets the reference (desired) velocity of the buoy, and (ii) a low level loop provides the required machinery (power take-off) force to achieve this velocity.

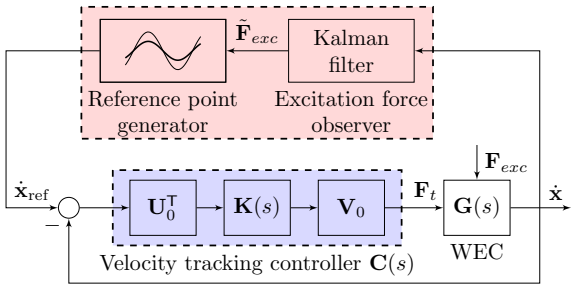

Figure 4: The block-diagram of the velocity tracking control designed for the three-tether WEC. In this paper, the 'tilde' symbol, ' ˜ ', denotes an estimated value of the variable.

3.1. High-level control

The main objective of the high-level controller is to set the reference buoy velocity, $\dot{\mathbf{x}}_{\text{ref}}$, having measured or estimated the wave excitation force, $\mathbf{F}_{exc}$. The controller does not require any predictions of the excitation force, only the current value should be provided. In Kracht et al. (2015), an observer has been designed to estimate the excitation force of a floating device based on the real-time measurements of its position, velocity, acceleration and control force. In this study, it is assumed that the current value of the wave excitation force is ideally estimated $\tilde{\mathbf{F}}_{exc}(t) = \mathbf{F}_{exc}^{\text{ideal}}(t)$ at each time step.

3.1.1. Surge-pitch compromise

According to the linear potential theory, the optimal velocity of the WEC that is able to absorb power from several degrees-of-freedom should satisfy the following equation (Falnes, 2002a):

$$\mathbf{B}(\omega)\hat{\dot{\mathbf{x}}}_{\text{opt}}(\omega) = \frac{1}{2}\hat{\mathbf{F}}_{exc}(\omega), \tag{12}$$

where the 'hat' symbol, ' ˆ ', denotes the complex amplitude, $\mathbf{B}(\omega) \in R^{6\times 6}$ is the matrix of radiation damping coefficients, $\hat{\dot{\mathbf{x}}}_{\text{opt}}(\omega) \in R^{6\times 1}$ is the vector of optimal velocity, and $\hat{\mathbf{F}}_{exc}(\omega) \in R^{6\times 1}$ is the excitation force vector. If $\mathbf{B}(\omega)$ is non-singular, then Equation (12) has a unique solution $\hat{\dot{\mathbf{x}}}_{\text{opt}}(\omega) = \frac{1}{2}\mathbf{B}^{-1}(\omega)\hat{\mathbf{F}}_{exc}(\omega)$. However, $\mathbf{B}^{-1}(\omega)$ does not exist for the axisymmetric body if surge and pitch are involved in power absorption, and Equation (12) cannot be solved simultaneously for $\hat{\dot{x}}_{1,\text{opt}}$ and $\hat{\dot{x}}_{5,\text{opt}}$. Therefore, if one of the velocities is known, the other one can be found from the following equation:

$$\begin{bmatrix} B_{11} & B_{15} \\ B_{51} & B_{55} \end{bmatrix} \begin{bmatrix} \hat{\dot{x}}_1 \\ \hat{\dot{x}}_5 \end{bmatrix} = \frac{1}{2} \begin{bmatrix} \hat{F}_{exc,1} \\ \hat{F}_{exc,5} \end{bmatrix}. \tag{13}$$

For instance, for the known value of the pitch velocity $\hat{\dot{x}}_5$, the optimal buoy velocity in surge can be calculated as in Falnes (2002b):

$$\hat{\dot{x}}_{1,\text{opt}} = \frac{\hat{F}_{exc,5} - 2B_{55}\hat{\dot{x}}_5}{2B_{51}} = \frac{\hat{F}_{exc,1} - 2B_{15}\hat{\dot{x}}_5}{2B_{11}}, \tag{14}$$

and vice-versa. So according to Equation 14, the requirement that the buoy velocity should be in phase with the excitation force does not apply if both surge and pitch modes are involved in power generation. For the number of cases considered in this paper, it is found that $\hat{F}_{exc,1} \gg 2B_{15}\hat{\dot{x}}_5$, and the coupling between surge and pitch is neglected in the design of the controller. In addition, due to the presence of the viscous damping force, the formulation of the optimal buoy velocity is modified as in Fusco and Ringwood (2013):

$$\hat{\dot{x}}_{1,\text{opt}} = \frac{\hat{F}_{exc,1}}{2(B_{11} + B_{v,1})}, \quad \hat{\dot{x}}_{3,\text{opt}} = \frac{\hat{F}_{exc,3}}{2(B_{33} + B_{v,3})}, \tag{15}$$

where $B_{v,1}$ and $B_{v,3}$ are linearised damping coefficients in surge and heave modes, respectively.

3.1.2. Causality assumption

The 'simple and effective' controller is based on the assumption that the wave excitation force has a narrow bandwidth which allows one to eliminate the complexity of the noncausal WEC control problem. Thus, the excitation force can be represented as a harmonic process with one dominant frequency as justified in Fusco and Ringwood (2013):

$$F_{exc,i}(t) \approx f_{exc,i}(t)\cos\big(\omega_i(t)t + \phi_i(t)\big), \tag{16}$$

where $f_{exc,i}(t)$, $\omega_i(t)$ and $\phi_i(t)$ are the time-variant amplitude, frequency and phase of the excitation force, respectively.

This assumption allows the reference velocity of the WEC in each hydrodynamic mode i to be set as:

$$\dot{x}_{i,\text{ref}}(t) = \frac{F_{exc,i}(t)}{2(B_{ii}(\tilde{\omega}_i) + B_{v,i})}, \tag{17}$$

where the estimated frequency $\tilde{\omega}_i$ is obtained in real time using the Extended Kalman filter (EKF) (Fusco and Ringwood, 2010) for each hydrodynamic mode i separately, and the corresponding value of $B_{ii}(\tilde{\omega}_i)$ is set using gain scheduling.

The unique feature of the fully submerged WECs is that they act as a bandpass filter being excited by the ocean waves in a limited range of wave frequencies. Therefore, the dominant frequency of the excitation force is different from the peak frequency of the incoming wave front.

The bandpass characteristics of the disk-like WEC considered in this study are shown in Figure 5a for the irregular wave of $H_s = 1$ m and $T_p = 14$ s. $S_\eta(\omega)$ corresponds to the Bretschneider wave spectrum (The Specialist Committee on Waves, 2002), $|H_{Fe,\eta}(\omega)|$ shows the magnitude of the transfer function from the wave elevation (η) to the heave excitation force, and $S_{Fe}(\omega) = S_\eta(\omega)|H_{Fe,\eta}(\omega)|^2$ demonstrates the resultant spectrum of the wave excitation force. So despite the fact that the incident waves have a peak frequency $\omega_p^\eta = 0.45$ rad/s (14 s), the peak excitation forces occur at a frequency of 0.6 rad/s (10.5 s). $\tilde{\omega}$ corresponds to the value estimated by the EKF.

The bandpass effect of the submerged WEC is clearly demonstrated in Figure 5b, where the horizontal axis shows to the peak wave period of the sea states of $H_s = 1$ m and the vertical axis shows the corresponding dominant period in the excitation force signal. Thus, for all the sea states with 9 s $< T_p <$ 17 s, the buoy oscillations in heave will be dominated by a period of 10 s.

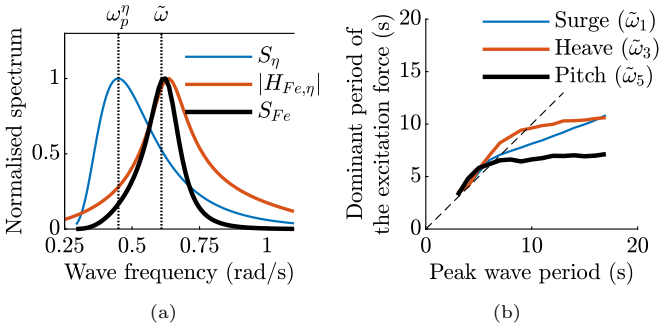

Figure 5: Bandpass properties of the three-tether WEC: (a) one sea state of $H_s = 1$ m and $T_p = 14$ s, (b) range of sea states with $H_s = 1$ m. Further details can be found in text.

3.2. Low-level control

As shown in Section 2.3, the three-tether WEC with a buoy shape considered in this study is a bad candidate for the inverse-based controllers due to the large condition number at the frequency range of interest. Therefore, as opposed to the internal-model approach implemented in Fusco and Ringwood (2013); Sergiienko et al. (2017), it was decided to use the SVD-controller for the tracking control loop (see Figure 4). This controller is proven to be robust (Skogestad and Postlethwaite, 2007) and allows one to decouple the control problem of the multivariable system:

$$\mathbf{C}(s) = \mathbf{V}_0\mathbf{K}(s)\mathbf{U}_0^\mathsf{T}, \tag{18}$$

where $\mathbf{V}_0$ and $\mathbf{U}_0$ are obtained from the singular value decomposition of $\mathbf{G}_0 = \mathbf{U}_0\mathbf{\Sigma}_0\mathbf{V}_0^\mathsf{T}$, $\mathbf{G}_0$ is a real approximation of $\mathbf{G}(j\omega_0)$ at a given frequency ω_0, and $\mathbf{K}(s) = K(s)\mathbf{\Sigma}_0^{-1}$. This controller only requires the design of $K(s)$ which is chosen as a simple PI controller: $K(s) = k_p + \frac{k_i}{s}$. In this study, $\omega_0 = 0.63$ rad/s, $k_p = 5$ and $k_i = 0$.

3.3. Controller performance

With the control structure defined, the performance of the SVD-based velocity tracking controller was investigated in terms of the reference tracking and power absorption properties.

3.3.1. Tracking

As demonstrated in Figure 6a–6b, the buoy velocity in both heave and surge has the same phase as the corresponding wave excitation force. As the pitch mode is not taken into account in the current controller design, it does not satisfy the phase optimality condition which is shown in Figure 6c. Therefore, the buoy oscillations in pitch have a negative impact on the power production that is demonstrated in Figure 6d. The power converted from each hydrodynamic mode j (surge, heave and pitch) is calculated as the difference between excitation power, radiated power and viscous losses: $\bar{P}_j = \bar{P}_{exc,j} - \bar{P}_{rad,j} - \bar{P}_{visc,j}$.

As a result, the power losses associated with the buoy motion in pitch constitute approximately 15% of the total amount of absorbed power.

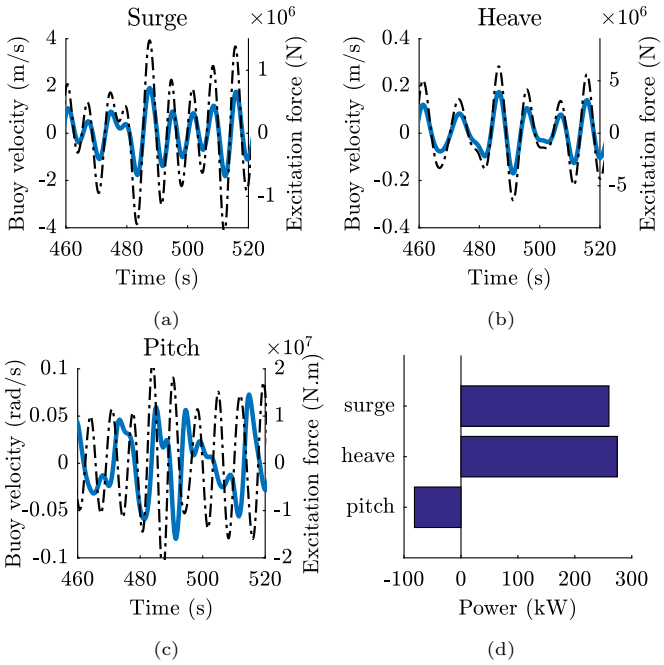

Figure 6: Time series of the buoy velocity (blue line) and the wave excitation force (black dash-dot-line) for the sea state of $H_s = 2$ m, $T_p = 12$ s: (a) surge, (b) heave, and (c) pitch modes. (d) The contribution of each hydrodynamic mode into the total power output of the three-tether WEC.

3.3.2. Comparison with a spring-damper control strategy

The performance of the proposed controller is compared with the commonly implemented spring-damper control (SDC) strategy, where the load force for the latter is defined as: $F_{u,i}(t) = -K_{pto}\Delta l_i(t) - B_{pto}\Delta\dot{l}_i(t), \quad i = 1\ldots3$. The control parameters K_{pto} and B_{pto} are optimised to maximise power output for each sea state using an exhaustive search.

The efficiency of both controllers is presented in Figure 7 for the range of sea states using Bretschneider wave spectra. The chosen SVD-based velocity tracking controller (VTC) is capable of increasing the power output of the three-tether WEC by up to 40% for $T_p > 8$ s, while for the wave periods of $T_p < 8$ s the spring-damper controller demonstrates slightly better results. This is mainly due to the linearisation of the SVD controller around ω_0 ($T_0 = 10$ s) frequency.

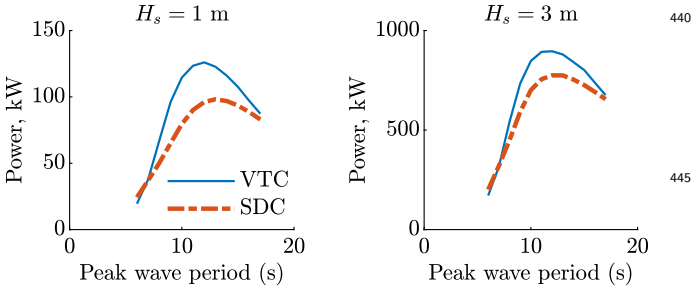

Figure 7: Performance comparison of the SVD-based velocity tracking control (blue solid line) vs. the spring-damper control (red dash-dot line) for the range of sea states generated using Bretschneider spectrum: (a) $H_s = 1$ m and (b) $H_s = 3$ m.

3.3.3. Sensitivity to the wave force estimation

WEC control systems aim to keep the buoy velocity in phase with the wave force. Modelling uncertainties and input/output disturbances may introduce errors in the reference and tracking loops leading to a significant degradation of the converter efficiency (O'Sullivan and Lightbody, 2017). For the controller shown in Figure 4, the main sources of modelling errors and their effect on the buoy performance are listed in Table 2. Firstly, the current value of the excitation force, $\tilde{\mathbf{F}}_{exc}(t)$, is estimated using the Extended Kalman filter which is based on the available model of the WEC. Any uncertainties in the WEC model could lead to the inaccurate estimation of the wave force (both amplitude and phase as in Kracht et al. (2015)), which, in turn, could lead to errors in setting the reference buoy velocity. Then, the estimated excitation force is passed to the reference point generator (Equation (17)) which uses the hydrodynamic damping, $B_{ii}(\omega)$, and linearised viscous damping, $B_{v,i}$, coefficients. Uncertainties in determining these values may introduce an error in setting the correct amplitude of the buoy velocity. The last 'known' modelling error is associated with the design of a velocity tracking control loop, in particular, inaccuracy in setting $K(s)$ and $\mathbf{\Sigma}_0$ values may lead to the tracking errors of the control system. This, in turn, may lead to the discrepancy between the desired (reference) and actual (measured) amplitude and phase of the buoy velocity.

In this study, it has been assumed that the perfect estimation of the wave excitation force is available, and the results presented in Figure 7 demonstrate the maximum capability of the velocity-tracking controller for the three-tether WEC. However, the information provided by the observer plays an essential role in this control strategy, and it is important to understand the effect of imperfect wave force estimation on the power output of the WEC.

Table 2: 'Known' modelling errors of the control structure shown in Figure 4.

Controller sub-system	Source of error	Buoy velocity Amplitude	Phase
Excitation force observer	WEC model	+	+
Reference point generator	$B_{ii}(\omega)$, $B_{v,i}$	+	
Velocity tracking loop	$K(s)$, $\mathbf{\Sigma}_0$	+	+

The sensitivity of the controller to the phase and amplitude errors of the estimated wave force is presented in Figure 8. To generate these results, it has been assumed that the force value used by the reference point generator has a time delay $\tilde{\mathbf{F}}_{exc}(t) = \mathbf{F}^{\text{ideal}}_{exc}(t-\tau)$ and the wave force amplitude error is modelled separately as $\tilde{\mathbf{F}}_{exc}(t) = (1+\varepsilon)\mathbf{F}^{\text{ideal}}_{exc}(t)$.

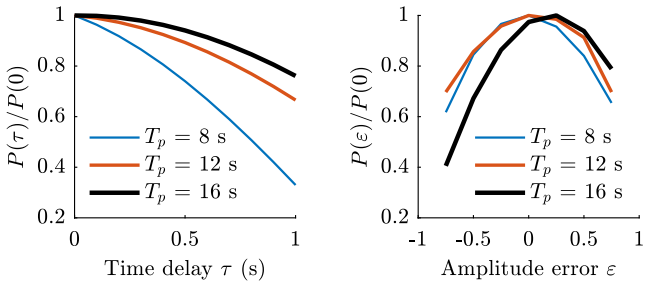

Figure 8: Sensitivity of the power output of the three-tether WEC to the imperfect estimation of the wave excitation force: (a) time delay, and (b) amplitude error.

As expected, the accurate estimation of the wave force phase is very important and the time delays of 0.3–0.7 s may result in power reduction of 20%. However, the system is more robust to the amplitude errors where uncertainties of ±50% in the estimation of the excitation force amplitude lead to a decrease in the generated power by only 20%. As a result, it should be realised that no matter how robust the velocity tracking loop is, the reference point generator is of greater importance, and to provide an accurate estimation of the wave forces it requires a high-fidelity model of the plant.

4. Considerations on practical application of the optimal control

The SVD-based velocity tracking control provides a significant increase in power absorption of the WEC. However, this efficiency comes at a cost of the PTO machinery since its specifications, such as the peak force, slew rate, energy storage, etc., directly depend on the implemented

control law. This section will specify what requirements the power take-off should meet in order to accommodate the close-to-optimal control strategy for the three-tether WEC.

4.1. Equivalent spring-damper control

The spring-damper controller is usually designed to operate on the sea-state basis, while the velocity tracking is a wave-by-wave control strategy. Thus, the question arises, assuming that the PTO can only operate as a spring-damper system, is it possible to implement the velocity-tracking control on such machinery using time-varying parameters $K_{pto}(t)$ and $B_{pto}(t)$? The results obtained for the regular wave of $H_w = 1$ m and T_w =10 sec are shown in Figure 9, where the required control force for each PTO unit of the three-tether WEC is calculated based on the VTC and then equivalent spring-damper parameters are estimated using the least-squares method:

$$K^{eq}_{pto,i}(t)\Delta l_i(t) + B^{eq}_{pto,i}(t)\Delta \dot{l}_i(t) := F^{VTC}_{u,i}(t), \quad i = 1, 2, 3. \tag{19}$$

The analysis is done assuming that the wave propagates along the x-axis ($\beta = 0°$) making the first tether aligned with an incoming wave front (refer to Figure 1).

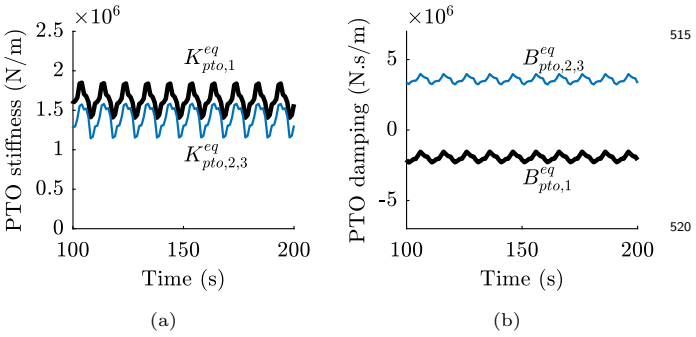

Figure 9: The time-dependent (a) stiffness and (b) damping coefficients of the equivalent spring-damper control for the regular wave of $H_w = 1$ m, $T_w = 10$ s.

The results imply that:

(i) in order to implement an optimal control on the three-tether WEC, all PTO units should have different settings $K^{eq}_{pto,1} \neq K^{eq}_{pto,2,3}$ and $B^{eq}_{pto,1} \neq B^{eq}_{pto,2,3}$;

(ii) the PTO attached to the first tether should act as an *actuator* not generating any power which is indicated by the negative value of the damping $B^{eq}_{pto,1} < 0$.

These findings are shown more clearly in Figure 10 for the range of irregular waves of $H_s = 1$ m. The contribution of each power take-off unit to the total power output of the three-tether WEC is shown for two different control strategies: velocity-tracking (Figure 10b) and spring-damper (Figure 10a). Power factor is calculated as the ratio of the power absorbed by one PTO to the total power absorbed by all three PTO systems ($\bar{P}_i / \sum \bar{P}_i$).

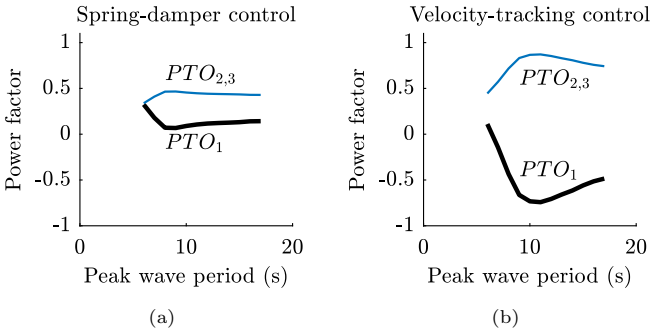

Figure 10: The contribution of each PTO unit to the total power absorption of the three-tether WEC depending on the sea state for two control strategies (a) spring-damper and (b) velocity tracking.

In the case of the spring-damper control considered here, all tethers have the same settings of the stiffness and damping, and these parameters are positive definite. As a result, all PTOs contribute to the power output, however the first unit generates much less energy than the other two as shown in Figure 10a. This is opposed to the velocity tracking control which requires the first PTO to act as an actuator across all sea states, while the power to the grid is delivered by the second and third PTOs. Similar observations have been reported in Scruggs et al. (2013) for the optimal causal control of the floating three-tether WEC. Moreover, this principle is also used in NEMOS NEMOS GmbHs (2017) wave energy converter, where one 'leg' is actuating the buoy motion according to the prescribed trajectory.

4.2. Wave direction

The results shown in Section 4.1 cover the scenario when the first tether is aligned with the wave propagation. However, the operational behaviour of each PTO unit (whether it operates as a generator or as an actuator) is highly dependent on the direction of the incoming wave. The effect of the wave angle β on the power factor of each PTO is demonstrated in Figure 11a for two different sea states. Thus, the operational behaviour of each PTO changes when waves come from the opposite direction ($\beta = 180°$): the first unit starts delivering power to the grid while the second and third PTOs serve as WEC actuators. Also it is interesting that for some wave angles (e.g. $\beta = 60°$), a single PTO needs to generate more power (power factor > 1) than the net power produced by the WEC.

Unlike the spring-damper controller, the velocity tracking control strategy is highly sensitive to the incident wave direction as illustrated in Figure 11a. Therefore, its performance in multidirectional waves can deteriorate significantly from the theoretical maximum subject to the directional spreading of the incoming wave. As a result, the three-tether WEC may benefit from the velocity tracking controller if installed close to the shore where the mean wave direction is highly predictable and the directional spreading does not exceed 10-20 degrees.

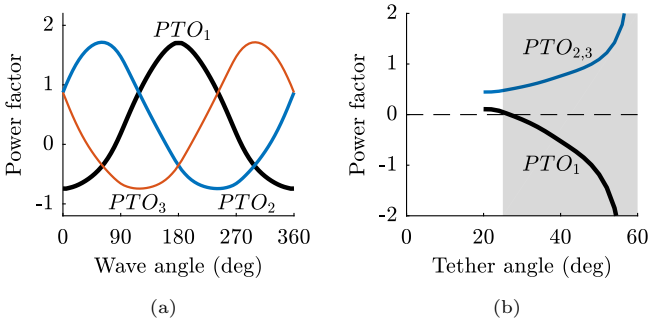

Figure 11: The effect of (a) the wave direction and (b) the tether inclination angle on the power factor of each PTO unit with implemented velocity tracking control for the sea state of $H_s = 1$ m, $T_p = 12$ s. Default settings of the WEC are specified in Figure 1.

4.3. Tether arrangement

The arrangement of tethers, including their inclination angles and attachment points, affect the power take-off capability of this WEC. As already mentioned in Section 2.1, the choice of the converter geometry and other parameters has been driven by minimisation of the levelised cost of electricity provided that the spring-damper control is implemented. Therefore, it is possible that the design of this WEC, in particular the tether arrangement, does not meet the requirements of the velocity-tracking controller. The effect of the tether angle α on the power factor of each PTO is demonstrated in Figure 11b for the sea state of $H_s = 1$ m and $T_p = 12$ s. It is clear that to be able to implement the velocity-tracking control on the three-tether WEC and to avoid the situation when one of the PTOs is working as an actuator, the tether angle should be reduced to approximately 25°. This can be explained by the fact that tethers and the PTO are trying to provide the required optimal motion of the buoy; and if the tether arrangement does not allow to achieve this trajectory with all PTOs generating power, then the optimal control pushes one or several PTO units to actuate the WEC instead of harvesting power.

More clearly the importance of the tether arrangement on the implementation of the optimal control can be shown by an example of the three-tether WEC with a different shape of the buoy (vertical cylinder with a radius of 3.8 m, height of 11.4 m, submergence depth of 3.75 m and water depth of 50 m). The new WEC and the power factors of its PTOs are demonstrated in Figure 12 for one sea state of $H_s = 1$ m and $T_p = 12$ s. It is obvious that for the tether angle close to $58 - 60°$, all three PTOs are generating useful power, while for the angles $< 55°$, the second and third PTOs are actuating the buoy motion (power factor is < 0). However, for larger tether angles the situation is completely opposite and to achieve an optimal trajectory of the buoy, the first PTO behaves as an actuator, whereas the second and third deliver electricity to the grid. It is important to note that only an axisymmetric arrangement of tethers is considered in this case study (all tethers have the same inclination angle to the vertical), while the possibility of other arrangements should be further investigated from a controllability point of view.

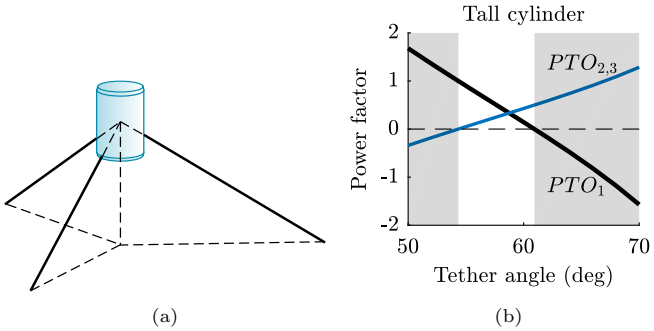

Figure 12: For demonstration purposes only: (a) a 3D view of the three-tether WEC with a cylindrical buoy of 3.8 m radius, 11.4 m height and submergence depth of 3.75 m; (b) power factor of each PTO depending on the tether arrangement assuming that $\alpha = \alpha_{AP}$ for the sea state of $H_s = 1$ m and $T_p = 12$ s.

As a result, the arrangement of tethers should be considered as an integral part of the control strategy and if it is not possible to install them according to the requirements, then the design of the PTO system should be modified appropriately.

4.4. Metrics

In order to implement a particular control strategy for the WEC, the PTO machinery should meet certain requirements. The analysis of the two control strategies is completed assuming a deployment site of Albany, Western Australia with a wave climate shown in Figure 13.

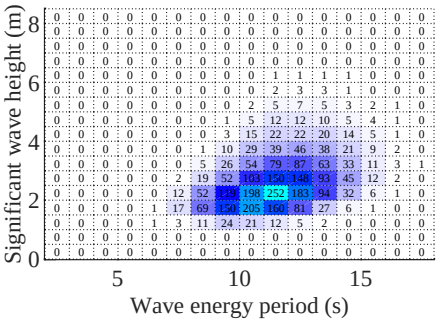

Figure 13: The wave climate at the Albany deployment site located in Western Australia (117.7547°E, 35.1081°S, 30 m water depth, 33.9 kW/m mean annual wave power resource) Australian Wave Energy Atlas (2017).

The quantities used to assess PTO specifications are adopted from Wilson et al. (2016) and indicated in Table 3. Values in bold are calculated assuming that all tethers are connected to the shared power take-off machinery $P(t) = \sum_{i=1}^{3} P_i(t)$, while values for individual power take-off systems correspond to the case when each tether is driving a separate isolated PTO unit.

Average net power for one sea state is calculated as $\bar{P} = \frac{1}{T}\int_T P(t)dt$ assuming a 100% efficiency of the actuator. Average reactive (input) power is estimated as

$\bar{P}^{in} = \frac{1}{T}\int_T P^{in}(t)dt$, where $P^{in}(t) = P(t)[P(t) < 0]$. The average stored energy is found as $\bar{E} = \frac{1}{N}\sum_{i=1}^{N} E_i$, where the energy stored for each cycle is calculated by integrating the reactive power between two consecutive zero crossings $E_i = \int_{t_{2i-1}}^{t_{2i}} P^{in}(t)dt$. A more detailed explanation of notations can be found in Figure 14. The average annual values reported in Table 3 are obtained taking into account the scatter diagram of wave statistics from Figure 13.

Table 3: Comparison of power production characteristics of two control strategies implemented on the three-tether WEC.

Performance index	Spring-damper control	Velocity tracking control
Average annual net power, kW	**496.0**	**567.4**
PTO 1	46.7	-171.2
PTO 2,3	224.7	369.3
Peak-to-average net power	**14.2**	**10.8**
Average annual reactive power, kW	**480.2**	**653.3**
PTO 1	122.3	1488.5
PTO 2,3	203.0	393.3
Peak-to-average reactive power	**3.9**	**5.6**
Average annual stored energy, kJ	**2393.3**	**1257.6**
PTO 1	655.4	5147.0
PTO 2,3	936.6	1561.0

As a result, the average annual power production for the velocity-tracking control is 15% higher than that for the spring-damper strategy. However, the negative value of the average net power for the PTO 1 confirms that this machinery should be designed to actuate the WEC all the time. The amount of energy required to provide the reactive power flow without using power from external sources is shown as 'average stored energy'. When all three PTO units have independent circuits (e.g. hydraulic), the VTC strategy involves much higher energy storage for each machinery, especially for PTO 1. However, it is more beneficial to design shared machinery, where power can flow between three PTO systems (e.g. inside the buoy), as this scenario allows the velocity-tracking controller to be implemented to the three-tether WEC with a reduction in energy storage costs as compared to the spring-damper control (1257.6 kJ vs. 2393.3 kJ).

5. Conclusion

The SVD-based velocity tracking control has been applied to the submerged multi-degree-of-freedom WEC. This controller is causal, robust, and achieves the optimal amplitude and phase between the buoy velocity and the excitation force in both heave and surge modes. The analysis of the controller sensitivity has revealed that while the low-level control loop is robust, the high-level reference point generator requires a high-fidelity model of the WEC in order to satisfy the optimal phasing condition. The performance of the proposed controller has been compared with a quasi-standard spring-damper approach, where a 15% increase in power production is achieved for the deployment site considered. It has been found that the velocity-tracking control implemented on the three-tether converter requires one of the PTO units to operate as an actuator all the time. However, this drawback can be compensated by the shared power take-off machinery across all the tethers.

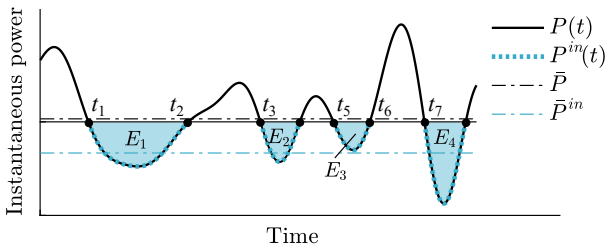

Figure 14: An example of calculating the power-production metrics for one time series. $P(t)$ is an instantaneous power, $P^{in}(t)$ is the input (reactive) power used to actuate the WEC, the 'bar' symbol $^-$ denotes the average value over time.

6. Acknowledgement

This research has been supported by the Australian Government Research Training Program Scholarship. The authors would like to thank Dr Ashkan Rafiee for providing the parameters of the WEC and the discussions of the results. Also, the assistance of Dr Giorgio Bacelli in calculating the power production measures is gratefully acknowledged.

References

References

Abdelkhalik, O., Zou, S., Robinett, R.D., Bacelli, G., Wilson, D., Coe, R.G., Korde, U.A., 2017. Multiresonant feedback control of a three-degree-of-freedom wave energy converter. IEEE Transactions on Sustainable Energy 8, 1518–1527.

Australian Wave Energy Atlas, 2017. URL: `http://nationalmap.gov.au/renewables/`. accessed 24 October 2017.

Bacelli, G., Balitsky, P., Ringwood, J.V., 2013. Coordinated control of arrays of wave energy devices - benefits over independent control. IEEE Transactions on Sustainable Energy 4, 1091–1099.

Coe, R.G., Bacelli, G., Wilson, D.G., Abdelkhalik, O., Korde, U.A., Robinett III, R.D., 2017. A comparison of control strategies for wave energy converters. International Journal of Marine Energy 20, 45–63.

Ding, B., Cazzolato, B.S., Arjomandi, M., Hardy, P., Mills, B., 2016. Sea-state based maximum power point tracking damping control of a fully submerged oscillating buoy. Ocean Engineering 126, 299–312.

Ding, B., Sergiienko, N., Meng, F., Cazzolato, B., Hardy, P., Arjomandi, M., 2019. The application of modal analysis to the design of multi-mode point absorber wave energy converters. Ocean Engineering 171, 603–618.

Faedo, N., Olaya, S., Ringwood, J.V., 2017. Optimal control, MPC and MPC-like algorithms for wave energy systems: An overview. IFAC Journal of Systems and Control 1, 37–56. doi:`https://doi.org/10.1016/j.ifacsc.2017.07.001`.

Falnes, J., 2002a. Ocean waves and oscillating systems: Linear interactions including wave-energy extraction. Cambridge University Press.

Falnes, J., 2002b. Solutions manual for problems on "Ocean waves and oscillating systems". Trondheim, Norway.

Folley, M., 2016. Numerical modelling of wave energy converters: State-of-the-art techniques for single devices and arrays. Elsevier Science, Saint Louis.

Fu, Z.F., He, J., 2001. Modal analysis. Butterworth-Heinemann.

Fusco, F., Ringwood, J.V., 2010. Short-term wave forecasting for real-time control of wave energy converters. IEEE Transactions on Sustainable Energy 1, 99–106.

Fusco, F., Ringwood, J.V., 2013. A simple and effective real-time controller for wave energy converters. IEEE Transactions on Sustainable Energy 4, 21–30.

Genest, R., Bonnefoy, F., Clément, A.H., Babarit, A., 2014. Effect of non-ideal power take-off on the energy absorption of a reactively controlled one degree of freedom wave energy converter. Applied Ocean Research 48, 236–243. doi:10.1016/j.apor.2014.09.001.

Hals, J., Falnes, J., Moan, T., 2011. A comparison of selected strategies for adaptive control of wave energy converters. Journal of Offshore Mechanics and Arctic Engineering 133, 031101–031101.

Hardy, P., Cazzolato, B.S., Ding, B., Prime, Z., 2016. A maximum capture width tracking controller for ocean wave energy converters in irregular waves. Ocean Engineering 121, 516–529. doi:http://dx.doi.org/10.1016/j.oceaneng.2016.05.045.

Korde, U.A., Lyu, J., Robinett, R.D., Wilson, D.G., Bacelli, G., Abdelkhalik, O.O., 2017. Constrained near-optimal control of a wave energy converter in three oscillation modes. Applied Ocean Research 69, 126–137. doi:https://doi.org/10.1016/j.apor.2017.10.004.

Kracht, P., Perez-Becker, S., Richard, J.B., Fischer, B., 2015. Performance improvement of a point absorber wave energy converter by application of an observer-based control: Results from wave tank testing. IEEE Transactions on Industry Applications 51, 3426–3434. doi:10.1109/TIA.2015.2405892.

Lee, C.H., 1995. WAMIT theory manual.

NEMOS GmbHs, 2017. The NEMOS Wave Energy Converter. URL: https://www.nemos.org/waveenergy/. accessed 31 October 2017.

Nie, R., Scruggs, J., Chertok, A., Clabby, D., Previsic, M., Karthikeyan, A., 2016. Optimal causal control of wave energy converters in stochastic waves - Accommodating nonlinear dynamic and loss models. International Journal of Marine Energy 15, 41–55. doi:https://doi.org/10.1016/j.ijome.2016.04.004.

O'Sullivan, A.C., Lightbody, G., 2017. The effect of model inaccuracy and move-blocking on the performance of a wave-to-wire wave energy converter, under economic predictive control, in: Proceedings of the 12th European Wave and Tidal Energy Conference, EWTEC. pp. 1012-1–1012-10.

Perez, T., Fossen, T.I., 2009. A Matlab toolbox for parametric identification of radiation-force models of ships and offshore structures. Modeling, Identification and Control 30, 1–15.

Rafiee, A., Fievez, J., 2015. Numerical prediction of extreme loads on the CETO wave energy converter, in: Proceedings of the 11th European Wave and Tidal Energy Conference, Nantes, France. pp. 09A1–2.

Ringwood, J.V., Bacelli, G., Fusco, F., 2014. Energy-maximizing control of wave-energy converters: the development of control system technology to optimize their operation. IEEE Control Systems 34, 30–55. doi:10.1109/MCS.2014.2333253.

Scruggs, J.T., Lattanzio, S.M., Taflanidis, A.A., Cassidy, I.L., 2013. Optimal causal control of a wave energy converter in a random sea. Applied Ocean Research 42, 1–15. doi:http://dx.doi.org/10.1016/j.apor.2013.03.004.

Sergiienko, N.Y., Cazzolato, B.S., Hardy, P., Arjomandi, M., Ding, B., 2017. Internal-model-based velocity tracking control of a submerged three-tether wave energy converter, in: Proceedings of the 12th European Wave and Tidal Energy Conference, pp. 1126-1–1126-8.

Sergiienko, N.Y., Rafiee, A., Cazzolato, B.S., Ding, B., Arjomandi, M., 2018. Feasibility study of the three-tether axisymmetric wave energy converter. Ocean Engineering 150, 221–233. doi:https://doi.org/10.1016/j.oceaneng.2017.12.055.

Skogestad, S., Postlethwaite, I., 2007. Multivariable feedback control: Analysis and design. volume 2. Wiley New York.

The Specialist Committee on Waves, 2002. Final report and recommendations to the 23rd ITTC, in: Proceedings of the 23rd International Towing Tank Conference, pp. 505–736.

Wilson, D., Bacelli, G., Coe, R.G., Bull, D.L., Abdelkhalik, O., Korde, U.A., Robinett III, R.D., 2016. A comparison of WEC control strategies. Technical report SAND2016-4293. Sandia National Laboratories.

Zou, S., Abdelkhalik, O., Robinett, R., Korde, U., Bacelli, G., Wilson, D., Coe, R., 2017. Model predictive control of parametric excited pitch-surge modes in wave energy converters. International Journal of Marine Energy 19, 32–46.